Alternating Flow in a Moving Corner

F. E. Laine-Pearson

University of Surrey, Guildford, GU2 7XH, UK

P. E. Hydon

University of Surrey, Guildford, GU2 7XH, UK

Abstract

Recent experiments have shown that rapid kinematic mixing occurs in the pulmonary alveoli. Here the Reynolds number is very small, there is recirculation in the alveolar cavity and the alveolar walls move periodically. We have recently shown that non-diffusing particles move chaotically in a two-dimensional model flow with the above features. In parts of the lung, however, there is asynchrony between the wall motion and the ductal flow immediately outside the alveolus. The extent to which this asynchrony affects kinematic mixing in real alveoli is not yet known. The purpose of this paper is to describe the effect of asynchrony on chaotic advection in our two-dimensional model, in order to understand the circumstances in which this becomes significant.

Keywords: Particle transport, Hamiltonian chaos, Physiological flows

PACS: 45.20.Jj, 47.52.+j, 05.45.Gg

Email addresses: f.laine-pearson@surrey.ac.uk (F. E. Laine-Pearson), p.hydon@surrey.ac.uk (P. E. Hydon)

1. Introduction

Experimental observations have demonstrated that rapid kinematic mixing occurs in the alveoli of the lung (11). These observations have prompted a major research program within the physiology community as they have implications for the transport of inhaled medicines and pollutants. In order to understand how kinematic mixing occurs, we use KAM (Kolmogorov-Arnol'd-Moser) theory to reveal a mechanism that is capable of producing substantial chaotic advection in cavities. KAM theory enables us to investigate questions about particle transport in alveolar flows that are hard to answer experimentally. In this paper, we examine one such question: to what extent does asynchrony between ductal flow and alveolar wall motion significantly affect mixing? We now describe the background to this problem.

Deep in the human lung there are hundreds of millions of alveoli (7). The flow occurring in these terminal air units, and in the ducts nearby that lead to these units, is incompressible and Newtonian. According to Haber *et al.* (2), the Reynolds number in alveoli is substantially less than 1. At normal breathing frequencies, the Womersley number is also considerably smaller than 1. Consequently alveolar and ductal flow can be regarded as Stokes flows.

There have been several flow studies in alveoli and their adjoining ducts. For this paper, three are particularly relevant. Tsuda *et al.* (10) constructed a numerical model of alveolar flow. They showed that recirculation can occur in an alveolus of sufficient depth. From these results, it was hypothesized that rotary mixing is an important part of mixing in the lung. To validate these computations, Tippe and Tsuda (9) constructed a mechanical model

to physically recreate flow in a model alveolus. They tracked particles, which led to results that supported their earlier findings. This evidence sparked a series of flow visualization experiments in rat lungs. Tsuda *et al.* (11) used liquid polymer in two colours to ventilate lungs slowly (to remain in a low Reynolds number regime), then fixed (solidified) the polymer after a small number of cycles. The flow pattern was revealed by taking sections; at no stage was significant blurring of the boundaries between colours observed, so any mixing was due to the flow rather than diffusion. After only half a breathing cycle, the mixing pattern was predominantly recirculatory in many alveoli. As ventilation continued, this initial pattern was disturbed; good mixing of fluid particles occurred after just a few breathing cycles.

Recently, we supported these findings by using Hamiltonian dynamical systems theory to describe a mechanism for the breakup of recirculating particle paths (3). We constructed a two-dimensional mathematical model based on a perturbation of the famous Moffatt corner eddies of fluid mechanics. These eddies are generated in corners whose angle is not too large (5); see Figure 1 for sample particle trajectories. At first sight, it may seem that flow in an alveolus will have little in common with flow in a sharp corner. However, each Moffatt eddy forms an isolated recirculation zone in which there are no sharp corners. A single main eddy of this type will occur in cavities of a wide range of shapes and sizes, provided that the aspect ratio is close to 1 (as is the case for mature alveoli). The precise geometry is less important than the qualitative features that cavity flows have in common. To simulate breathing, we added a periodically expanding and contracting wall motion. Our results were quite striking: the interaction of recirculation and wall

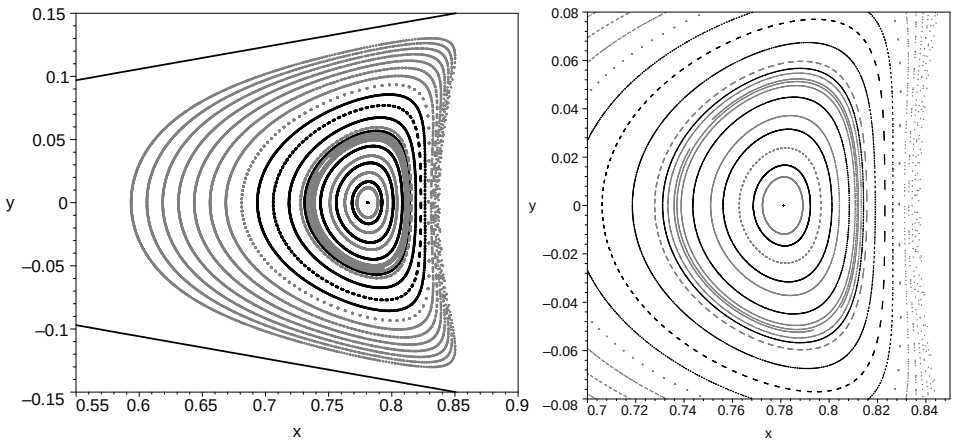

Figure 1: A region of recirculating flow in a corner. The parameter values (see §2) are $2\phi_0 = 20°, K_0 = 0.25, K_1 = 0$ and $\epsilon = 0$. **Left:** Eight closed trajectories are coloured black, while the other sixteen are coloured grey. (This is to differentiate between particle trajectories when the flow is perturbed.) The flow is steady, so particle paths follow streamlines, creating closed orbits; see (3) for more details. **Right:** Enlargement of the centre of the recirculating region.

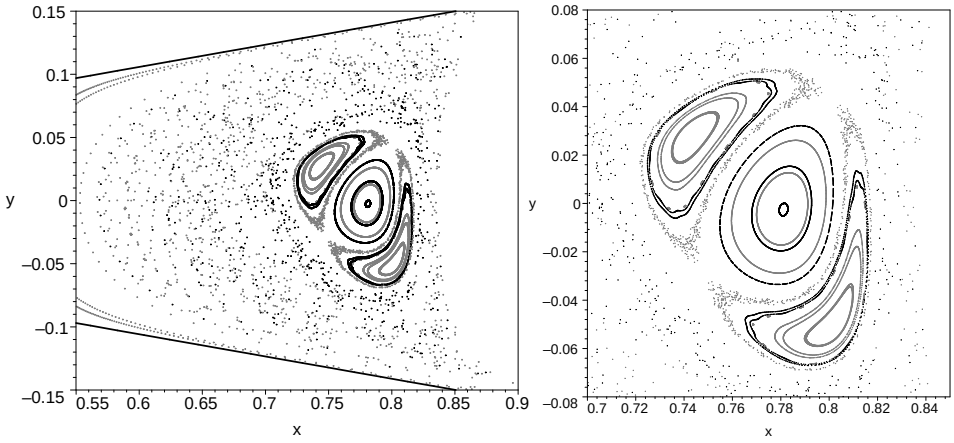

Figure 2: Poincaré section showing particle motion when the walls in Figure 1 expand and contract periodically; see (3) for details. The parameter values (see §2) are $2\phi_0 = 20°, K_0 = 0.25, K_1 = 0$ and $\epsilon = 0.005$. **Left**: A small (0.5%) periodic perturbation of the wall angle produces a striking effect on trajectories. **Right**: Some KAM tori remain, but they are surrounded by a sea of chaos.

movement provided us with a picture of chaotic regions of particle transport coexisting amongst regular paths. Figure 2 illustrates this remarkable structure when the parameter controlling wall movement is very small. To explain this picture, we shall briefly introduce some terminology. A 'Poincaré section', is constructed by marking the position of a particle periodically. Here this corresponds to plotting a single point per trajectory after each breathing cycle. We will call the flow driven by the wall motion alone 'squeeze flow' and we shall refer to the recirculating flow as 'Moffatt flow'. Put simply, when these two flows are combined the squeeze flow competes with the Moffatt flow. As the corner is approached, the squeeze flow dominates, allowing a particle's path to average that of a steady eddy. Moving far away from the

corner, the Moffatt flow dominates and most particles recirculate. There is an intermediate region where the magnitude of the squeeze flow is comparable with that of the Moffatt flow. It is here that a particle may move regularly or chaotically within a well-defined self-similar structure. As amplitude of the wall motion increases, so does the total area of chaos. Chaotic transport is maximized within the intermediate area, thereby enhancing mixing of particles. In pure Moffatt flow, particles recirculate on closed trajectories. There are some remnants of these trajectories in the chaotic flow. They appear to be closed orbits (provided one plots the position of particles that lie on them for enough cycles); these orbits are called 'KAM tori'.

Throughout this paper, we restrict attention to particles that are advected and do not diffuse substantially during a few breathing cycles. This is consistent with the above experiments; it is also relevant to the transport of small inhaled particles that have little inertia. It does not apply to the mixing of inhaled gases. There are many other factors that can affect particle transport deep in the lung. We investigate one of these, namely, asynchrony between the ductal flow and the motion of the walls. Asynchrony occurs for various reasons (such as the location of the alveoli and the state of health of the lung). We model it by including a phase shift in our two-dimensional Moffat/squeeze flow model. Our results give a qualitative picture of the extent to which asynchrony affects particle transport in the model. It seems reasonable to conclude that if asynchrony produces a small (or large) effect in the two-dimensional model, it will do much the same in a real alveolus. (Of course, because of the move from two to three dimensions, the extent of chaotic advection in an alveolus may be very different to that in our model.)

In §2 the flow field is constructed. The equations of motion for particle transport are described as a time-dependent Hamiltonian system in §3. Results for the basic model of Moffatt eddies in a moving corner are reviewed. A physical description of the alternating flow model is given in §4, and used to explain our qualitative results. We discuss the effects of varying parameters and explain the physical mechanisms in the context of real alveoli.

2. Constructing the Flow Field

Throughout this paper, we use carets to denote dimensional variables; these are removed when variables are non-dimensionalized.

Consider Stokes flow of a fluid bounded by a corner whose walls oscillate, with an alternating flow occurring far from the corner. When the walls are not moving and the far-field flow is unidirectional, an infinite stream of eddies is induced in the corner for angles of less than $2\phi_{\text{critical}} = 146.3°$; this model was formulated by Moffatt (5).

We consider what happens when the (steady) Moffatt flow is perturbed by the squeeze flow and an alternating far-field flow, incorporating a phase shift. We require that the maximum angle of the corner remains less than $2\phi_{\text{critical}}$. Let $\hat{\mathbf{u}} = \hat{u}_{\hat{r}}\mathbf{e}_{\hat{r}} + \hat{u}_{\theta}\mathbf{e}_{\theta}$ be the velocity field with respect to (steady) plane polar coordinates $(\hat{r}, \theta)$. The incompressibility condition is

$$\frac{1}{\hat{r}}\left(\hat{r}\hat{u}_{\hat{r}}\right)_{,\hat{r}} + \frac{1}{\hat{r}}\left(\hat{u}_{\theta}\right)_{,\theta} = 0.$$

The corner region is simply-connected, so there exists a streamfunction $\hat{\psi}(\hat{r}, \theta, \hat{t})$ such that $\hat{u}_{\hat{r}} = \hat{\psi}_{,\theta}/\hat{r}$ and $\hat{u}_{\theta} = -\hat{\psi}_{,\hat{r}}$. As the flow is a Stokes flow, the stream-

function satisfies the biharmonic equation,

$$\hat{\nabla}^4\hat{\psi} \equiv \left(\frac{\partial^2}{\partial\hat{r}^2} + \frac{1}{\hat{r}}\frac{\partial}{\partial\hat{r}} + \frac{1}{\hat{r}^2}\frac{\partial^2}{\partial\theta^2}\right)^2 \hat{\psi} = 0.$$

The walls are moving and are at $\theta = \pm\phi$, where $\phi = \phi_0[1 + \epsilon\sin(\omega\hat{t})]$; here $2\phi_0$ is the mean corner angle, ω is the frequency of oscillation and $0 \leq \epsilon \ll 1$. Consequently the boundary conditions are

$$\hat{\psi}_{,\theta} = 0, \quad \hat{\psi}_{,\hat{r}} = \mp\epsilon\phi_0\omega\hat{r}\cos(\omega\hat{t}) \quad \text{on} \quad \theta = \pm\phi.$$

To non-dimensionalize, let

$$t = \frac{\omega\hat{t}}{2\pi}, \quad r = \frac{\hat{r}}{a}, \quad \psi = \frac{\hat{\psi}}{a^2\omega},$$

where a is a convenient length scale. (We shall explain our choice of a once we have written down the streamfunction ψ.)

It is helpful to split the streamfunction into two parts, $\psi = \psi_M + \psi_W$, where each part solves the nondimensionalized biharmonic equation. Here ψ_M is the streamfunction for the instantaneous Moffatt flow, which is driven by the flow outside the corner (the far-field flow) and satisfies homogeneous boundary conditions at the walls. The given boundary conditions are satisfied by ψ_W, which generates the squeeze flow.

We now summarise the key features of Moffatt flow; for further details, readers should consult Moffatt (5). The solution of the biharmonic equation with homogeneous boundary conditions $\psi_{M,r} = \psi_{M,\theta} = 0$ on the walls is an infinite series of eigenfunctions. The leading terms produce Moffatt flow; these correspond to the dominant complex eigenvalues λ and $\bar{\lambda}$ (namely, the pair of eigenvalues with smallest positive real part). The Moffatt streamfunc-

tion is well-known; for our purposes, the following form of it is convenient:

$$\psi_M(r,\theta,t) = \mathrm{Re}\left\{Kr^\lambda[\cos((\lambda-2)\phi)\cos(\lambda\theta) - \cos(\lambda\phi)\cos((\lambda-2)\theta)]\right\}. \quad (1)$$

Here the amplitude K is a measure of the strength of the far-field driving flow. The homogeneous boundary conditions on the walls require that λ is related to ϕ by

$$\sin(2\phi\mu) = -\mu\sin(2\phi), \quad \text{where} \quad \mu = \lambda - 1. \quad (2)$$

From Moffatt (5), the dominant eigenvalue λ can be written

$$\lambda = \left(1 + \frac{\xi}{2\phi}\right) + i\left(\frac{\eta}{2\phi}\right),$$

where $\xi \approx 4$ and $\eta = O(1)$.

In our problem the angle ϕ is a function of t, so λ is also time-dependent. We set the amplitude to be

$$K = K_0 + K_1\sin(2\pi t + \delta), \qquad K_j \geq 0, \quad j = 0, 1,$$

which corresponds to a far-field with a steady component (K_0) and an oscillatory component (K_1) with a phase shift δ. (If $K_1 = 0$, the flow reduces to the one considered in (3); if $K_0 = 0$, the flow is purely oscillatory.)

The inhomogeneous boundary conditions for the total streamfunction ψ are satisfied by ψ_W; they are

$$\psi_{W,r} = \mp\epsilon r\phi_0\cos(2\pi t), \qquad \psi_{W,\theta} = 0 \qquad \text{when} \quad \theta = \pm\phi.$$

The particular solution of the biharmonic equation that satisfies these conditions is

$$\psi_W(r,\theta,t) = -\epsilon\phi_0\left(\frac{r^2}{2}\right)\cos(2\pi t)\left[\frac{\sin(2\theta) - 2\theta\cos(2\phi)}{\sin(2\phi) - 2\phi\cos(2\phi))}\right]. \quad (3)$$

The squeeze flow and the modification to Moffatt flow caused by the wall motion combine to produce an $O(\epsilon)$ perturbation to the steady Moffatt flow. The two components of the perturbation are proportional to different powers of $\hat{r}$. We choose a to be the length scale at which these components are of comparable size, so that this occurs for $r = O(1)$.

3. Transport of Passive Particles

Particle trajectories are obtained from the Lagrangian equations of motion

$$\frac{1}{2\pi}\frac{\mathrm{d}r}{\mathrm{d}t} = \frac{1}{r}\frac{\partial\psi}{\partial\theta}, \quad \frac{1}{2\pi}\frac{\mathrm{d}\theta}{\mathrm{d}t} = -\frac{1}{r}\frac{\partial\psi}{\partial r}.$$

By introducing $R = r^2$, these equations can be written as a Hamiltonian system for R and θ,

$$\frac{\mathrm{d}R}{\mathrm{d}t} = -\frac{\partial H}{\partial\theta}, \quad \frac{\mathrm{d}\theta}{\mathrm{d}t} = \frac{\partial H}{\partial R}, \tag{4}$$

where the Hamiltonian H is

$$H(R,\theta,t) = -4\pi\psi(R^{1/2},\theta,t).$$

In the absence of wall motion, when the far-field motion is unidirectional, the Hamiltonian is

$$H_0(R,\theta) = -4\pi\left[\psi_M(R^{1/2},\theta,t)\right]_{\epsilon=K_1=0}.$$

In this case the flow is steady, so particles will stay on the streamlines; these are curves of constant H_0, which do not change with time. Hence the system

$$\frac{\mathrm{d}R}{\mathrm{d}t} = -\frac{\partial H_0}{\partial\theta}, \quad \frac{\mathrm{d}\theta}{\mathrm{d}t} = \frac{\partial H_0}{\partial R},$$

is integrable; there exist action-angle coordinates in terms of which the flow on each streamline is a steady rotation.

Moreover, the amplitude K does not affect the streamline pattern; it only governs the rate at which particles go around the streamlines. Thus even if K_1 is nonzero, making the flow unsteady, the particles will remain on curves of constant H_0. If $K_0 = 0$, however, the particles will just oscillate back and forth; their trajectories may or may not be closed. Wherever the Moffatt flow (whether steady or not) produces closed trajectories, these can be perturbed into chaos by the wall motion. So the amplitude of the wall motion, ϵ, is the key perturbation parameter.

Figure 1 shows typical particle paths when $2\phi_0 = 20°$, $K_0 = 0.25$, $\epsilon = 0$ and $K_1 = 0$. This illustration has been generated by integrating the equations of motion (4) using an explicit fourth-order Runge-Kutta scheme with a step size of 0.01; a point has been plotted at $t = 0, 1, 2, \ldots, 1000$. The initial conditions are spaced out along the line $y = 0$ and positioned at $x = c_E + 0.0125(j - 16)$ where c_E is the centre of the eddy and $j = 1, 2, \ldots, 16$. An additional eight initial conditions have been evolved to enhance the view later when $\epsilon \neq 0$; they are positioned at $(x, y) = (0.74 + 0.0125(k - 1), 0.01)$ and $(x, y) = (0.77 + 0.0125(k - 1), -0.05)$ for $k = 1, 2, 3, 4$. This eddy has been chosen specifically as, when $\epsilon \neq 0$ and $K_1 \neq 0$, it lies in the intermediate area where the squeeze flow is of the same order of magnitude as the Moffatt flow. Consequently, it is an ideal representative for observing the qualitative behaviour of particles when the system is perturbed.

For the moving corner and alternating far-field flow, the Hamiltonian is

$H = H_0 + H_1$, where

$$H_1(R, \theta, t) = -4\pi\psi_M(R^{1/2}, \theta, t) - 4\pi\psi_W(R^{1/2}, \theta, t) - H_0(R, \theta).$$

The function H_1 vanishes as $\epsilon \to 0$ and $K_1 \to 0$. Formally, the part of H_1 that depends on the wall motion is of $O(\epsilon)$ provided that $\lambda = \lambda_0(1 + O(\epsilon))$, where λ_0 is obtained by solving relation (2) when the corner is fixed with angle $2\phi_0$.

The Hamiltonian H has been constructed in this way so that KAM theory can be applied. The classical KAM theorem is concerned with proving the persistence of closed orbits of Hamiltonian systems that can be written as an integrable Hamiltonian system plus a non-integrable perturbation, controlled by a perturbation parameter that is much smaller than 1; these are called 'near-integrable Hamiltonian systems'. In our problem H_0 is integrable, while H_1 consists of two parts. The oscillatory amplitude K_1 does not break integrability, but it may stop recirculation occurring in some places; the wall motion is the non-integrable perturbation, controlled by the parameter ϵ. Simply put, the KAM theorem says that many of the closed orbits appearing in Figure 1 will persist (though may deform) as long as the perturbation parameter ϵ is sufficiently small; such orbits lie on so-called 'KAM tori', which look like solid curves in Poincaré sections. Although the theorem was originally proved by assuming that the perturbation is exponentially small, some KAM tori remain even when the perturbation parameter is $O(1)$; then the surrounding chaotic region tends to be large. A good introduction to this topic can be found in Tabor (8), with a more detailed explanation in Lichtenburg and Lieberman (4).

Figure 2 illustrates what happens to the particle paths of Figure 1 when

$\epsilon = 0.005$ ($2\phi_0 = 20°$, $K_0 = 0.25$, $K_1 = 0$); similar illustrations (for various ϵ) can be found in (3). This Poincaré section has been constructed by plotting particle positions at $t = 0, 1, 2, \ldots, 1000$. Here, we can see that the innermost curves in Figure 1 have survived the perturbation (albeit skewed).

However, KAM theory does not account for the behaviour of particles belonging to the curves that do not survive. These curves can break up in a number of ways. The particles of the unperturbed system with frequencies that resonate with the frequency of the perturbed system are the origin for the islands that have formed — this is in accordance with the Poincaré-Birkhoff Fixed-Point theorem. (Figure 2 clearly shows a chain of two such islands.) Other particles, that neither resonate with the perturbed system nor satisfy the requirements of the classical KAM theorem, may move around in chaotic regions. (This occurs for the outermost curves of Figure 1 — they are replaced by the haze of points in Figure 2, which illustrates this phenomenon.) Further details regarding these behaviours can be found in the literature; for instance, see (4; 8). The overall structure can be classed as 'self-similar', which means that the occurrence of islands, regular curves and chaotic regions appear on all scales. Enlarging any island would show that it is made up of island chains of its own.

4. Results

A circulatory motion is generated by rotating the fluid far from the corner. For a unidirectional flow with $K_1 = 0$, particles circulate around closed orbits which form Moffatt eddies (5). When $K_1 \leq K_0$, the far-field flow is periodically varying in speed but it does not change direction; it is still

a unidirectional flow. To mimic the movement of air past alveoli during breathing cycles, we choose the far-field flow so that it is bidirectional and oscillatory, by setting $K_1 > K_0$. When $K_0 = 0$ but $K_1 \neq 0$, a particle will return to its initial position after every cycle; in a Poincaré section, we would see a single point for each particle. When $K_0 \neq 0$, particles generically do not ever return to the same position. Instead, the points on the Poincaré section that mark a particle's trajectory are dense in a closed curve that is close to the corresponding orbit when $K_1 = 0$. This is the basic recirculation pattern.

When we incorporate a periodically expanding and contracting wall motion into the basic set-up, this produces chaos, as seen in the right-hand Poincaré sections of Figure 3.

When $K_1 = \epsilon = 0$, only K_0 will affect how fast a particle will move around the eddy shown in Figure 1 ($2\phi_0 = 20°$, $K_0 = 0.25$); increasing K_0 will increase the speed of a particle. According to Moffatt (5), there is an infinite stream of eddies into the corner, so the chosen eddy of Figure 1 will be sandwiched between two neighbouring eddies; its nearest neighbours are illustrated in (3) for various ϵ. The neighbour to the left is dominated by the squeeze flow, whereas the right-hand neighbour is dominated by the (adapted) Moffatt flow. This is because the strength of each eddy is approximately 380 times weaker than its right-hand neighbour for a corner of angle 20°; see (5) for calculations. The eddy pictured in Figure 1 lies in the intermediate area where the squeeze flow is a small perturbation to the Moffatt flow. By fixing $\epsilon \neq 0$, increasing K_0 causes more KAM tori to break up; see Figure 3 (top-left) for $K_0 = 0.125$, Figure 2 (left) for $K_0 = 0.25$ and Figure

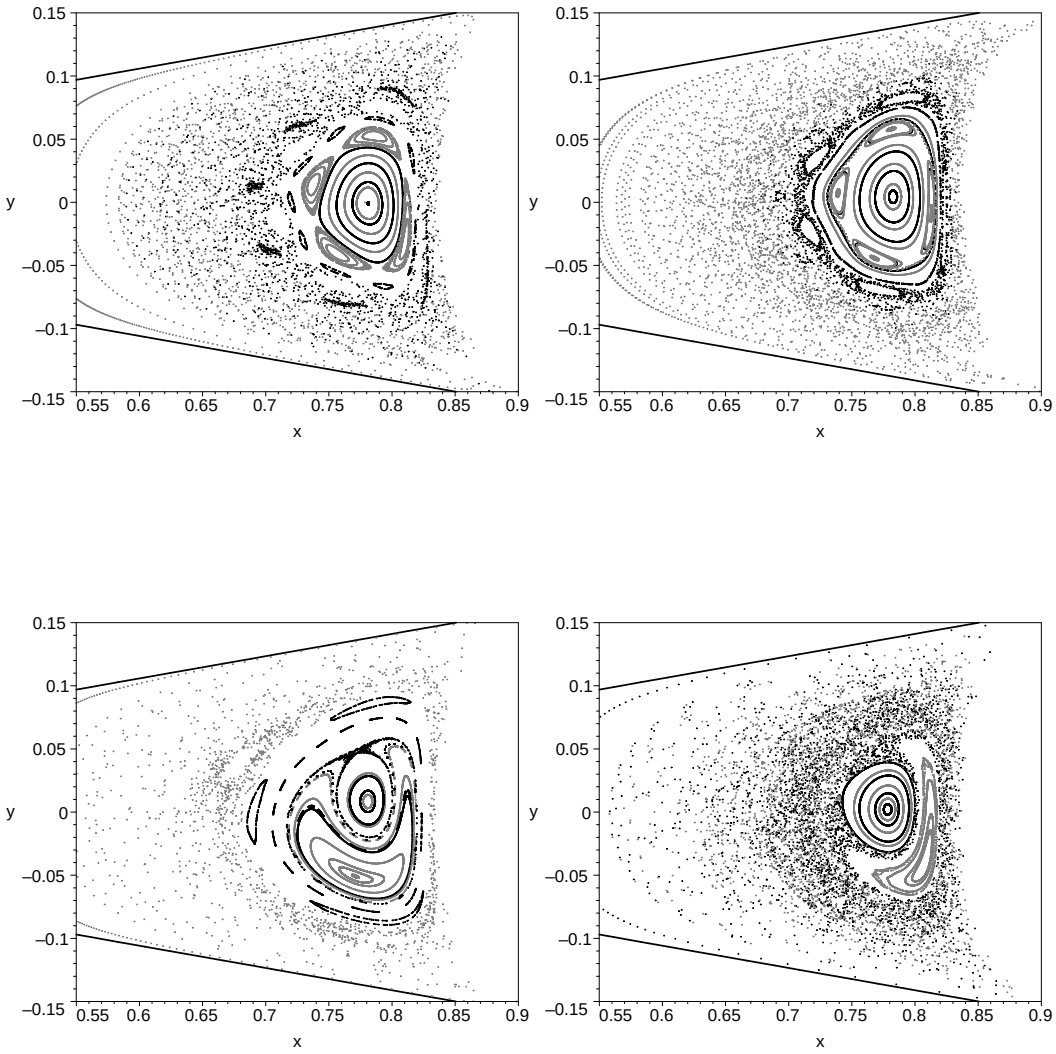

Figure 3: Poincaré sections of particle motion when $2\phi_0 = 20°$, $\epsilon = 0.005$, with $\delta = 0°$. The eight main trajectories are shown in black, while the additional set of 16 trajectories are coloured grey. **Top:** $K_0 = 0.125$; $K_1 = 0$ (left) and $K_1 = 0.5$ (right). **Bottom:** $K_0 = 0.5$; $K_1 = 0$ (left) and $K_1 = 0.5$ (right).

3 (bottom-left) for $K_0 = 0.5$.

Let us now examine the qualitative structure when ϵ, K_0 and K_1 are non-zero. Figure 3 (top) shows that a weak unidirectional contribution does not cause the self-similar structure to change much, even when the periodically alternating contribution is much stronger. For a sufficiently strong K_0, increasing K_1 will enlarge the outer chaotic region; see Figure 3 (bottom). This corresponds to increased mixing of particles. Note that in Figure 3 (bottom-right), $K_0 = K_1 = 0.5$ and therefore the flow is technically still unidirectional.

The effect of asynchrony, through the phase shift δ, is amplified given sufficiently strong K_1; compare Figure 4 with Figure 5. Increasing δ causes the self-similar structure to rotate clockwise, which is the direction a particle moves on the eddy when $\epsilon = K_1 = 0$. This is more noticeable in Figure 5. Also, the main chain of islands (located around the central region of regular curves) adapt in shape as the phase shift changes, but some of the self-similar structure remains (in a qualitative sense). When the wall motion and the alternating far-field motion oppose one another ($\delta = 180°$), the self-similar structure appears strengthened, by which we mean that a somewhat larger area is occupied by KAM tori. This can be seen by comparing either Figure 5 (top-left) with Figure 6 (right) or, better still, Figure 4 (top-left) with Figure 6 (left). The former example has $K_1 > K_0$, whereas the latter example has $K_1 < K_0$.

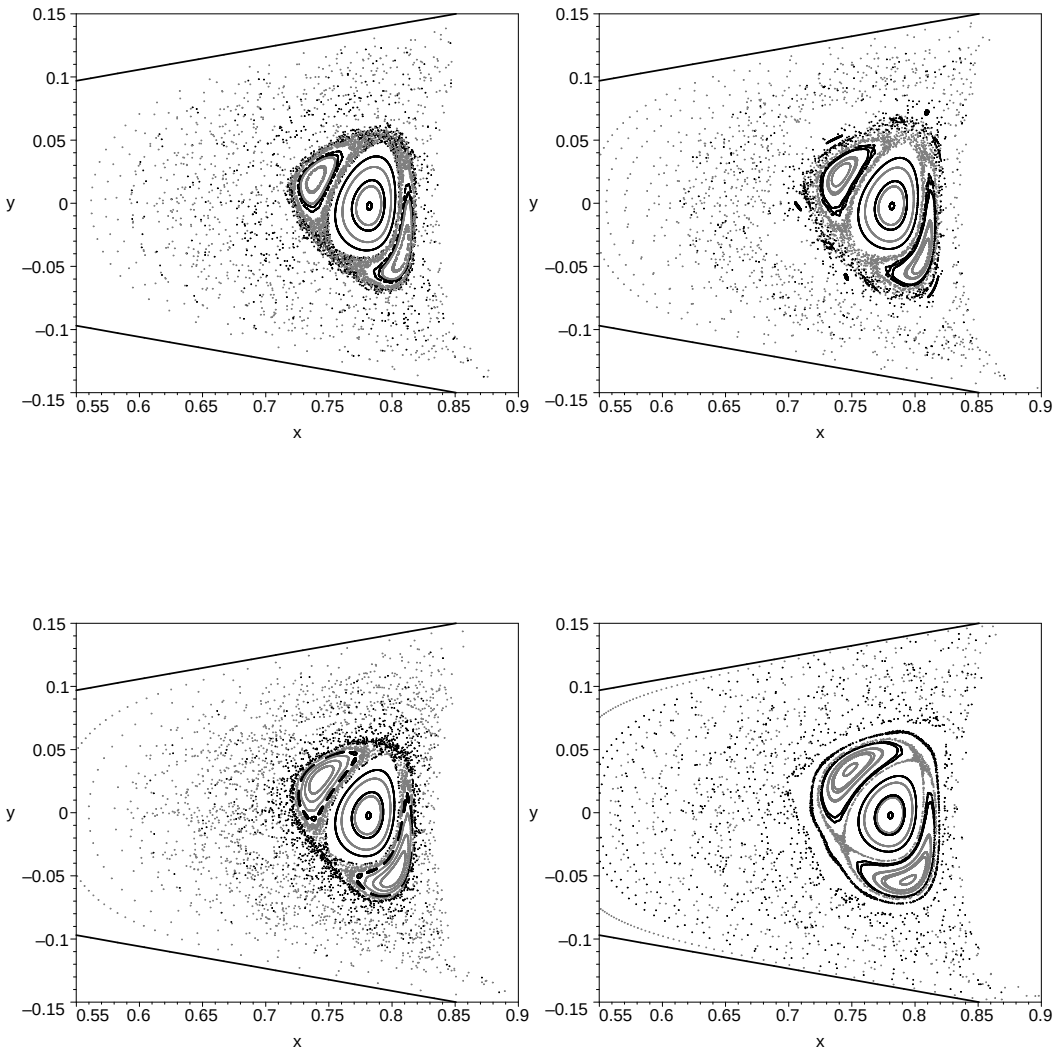

Figure 4: Poincaré sections of particle motion when $2\phi_0 = 20°$, $K_0 = 0.25$, $\epsilon = 0.005$, with $K_1 = 0.125$. The eight main trajectories are shown in black, while the additional set of 16 trajectories are coloured grey. **Top-Left:** $\delta = 0°$. **Top-Right:** $\delta = 50°$. **Bottom-Left:** $\delta = 75°$. **Bottom-Right:** $\delta = 125°$.

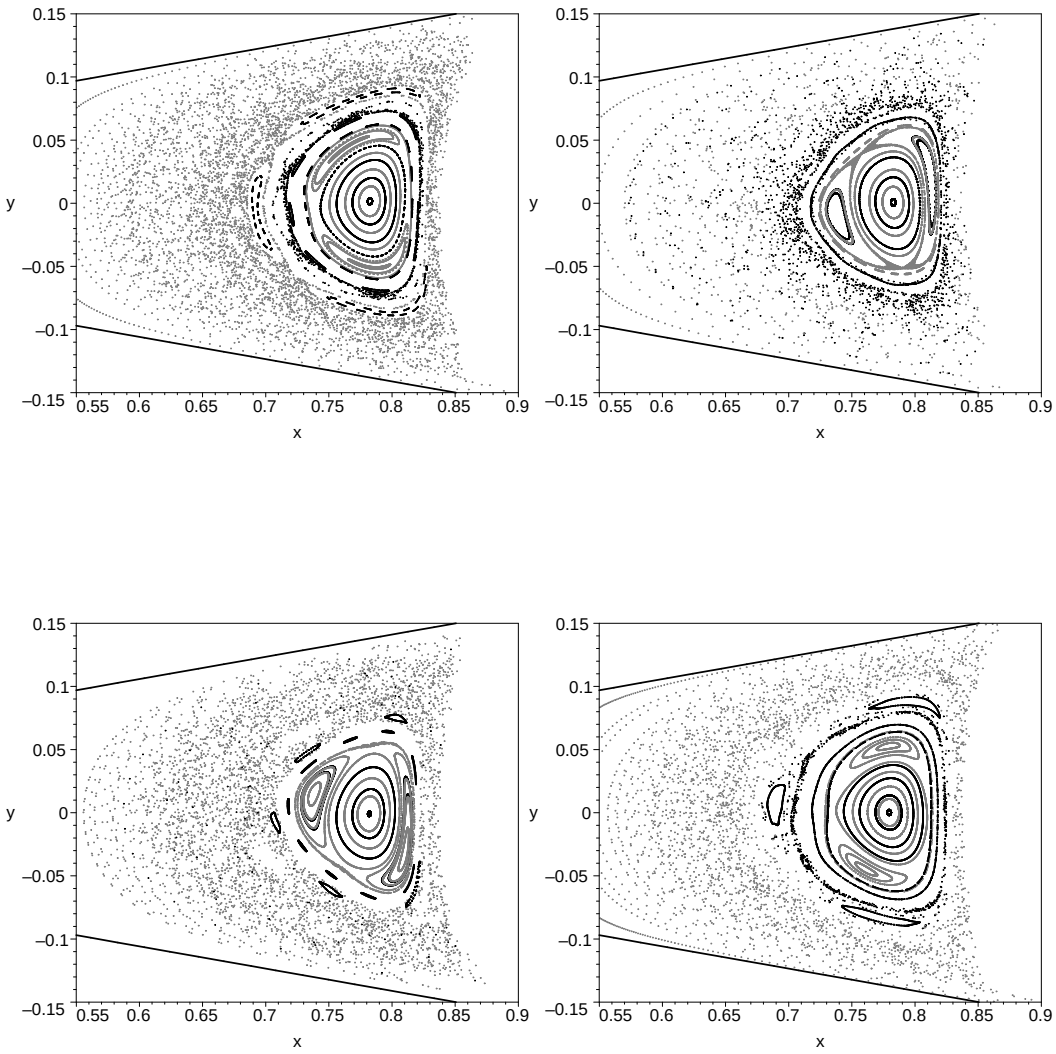

Figure 5: Poincaré sections of particle motion when $2\phi_0 = 20°$, $K_0 = 0.25$, $\epsilon = 0.005$, with $K_1 = 0.5$. The eight main trajectories are shown in black, while the additional set of 16 trajectories are coloured grey. **Top-Left:** $\delta = 0°$. **Top-Right:** $\delta = 50°$. **Bottom-Left:** $\delta = 75°$. **Bottom-Right:** $\delta = 125°$.

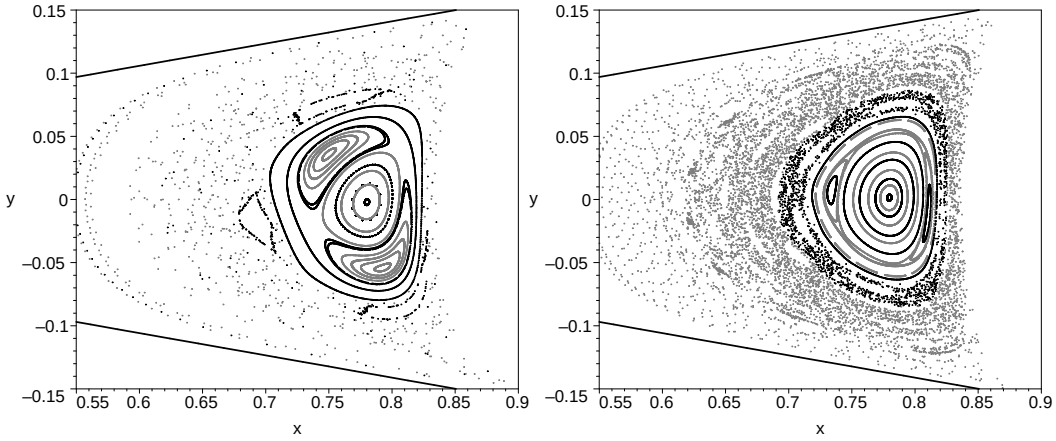

Figure 6: Poincaré sections of particle motion when $2\phi_0 = 20°$, $K_0 = 0.25$, $\epsilon = 0.005$, with $\delta = 180°$. The eight main trajectories are shown in black, while the additional set of 16 trajectories are coloured grey. **Left:** $K_1 = 0.125$. **Right:** $K_1 = 0.5$.

5. Discussion and conclusions

We now discuss the physiological relevance of our mathematical model. Real alveolar flows are three-dimensional. So it is reasonable to ask whether our two-dimensional model can provide some insight. Tsuda *et al.* (11) showed that recirculation can occur in alveoli, provided they are sufficiently deep. Additionally, the results of Laine-Pearson and Hydon (3) suggest that, in places where the squeeze flow is of the same order of magnitude as recirculation, some particles move chaotically. Our new results, which use the more physiologically-realistic bidirectional far-field flow ($K_1 > K_0$) instead of a constant unidirectional far-field flow ($K_1 = 0$), reinforce this observation. Moreover, the addition of sufficiently large enough alternating component slightly enlarges the self-similar region. Adding a phase difference controls the extent of chaos further. Deep in the lung, the asynchrony is normally

quite small (2). Therefore the phase shift would probably only affect the flow in the alveoli marginally, possibly just rotating the self-similar structure.

Our results cannot be used to deduce whether chaotic motion occurs at the edges of the alveoli, because there the Moffatt flow is a perturbation to the squeeze flow. However, they are relevant for the majority of the volume of each cavity.

To conclude, for weakly-varying unidirectional flow ($K_1 < K_0$), the self-similar structure hardly changes from when the unidirectional flow is constant ($K_1 = 0$); compare Figure 4 (top-left) with Figure 2 (left). For oscillatory bidirectional flow ($K_1 > K_0$), the self-similar structure appears to enlarge; compare Figure 3 (top-right) with Figure 3 (top-left) or Figure 5 (top-left) and Figure 2 (left). However, when both the alternating and unidirectional contributions to the far-field flow are sufficiently large and similar in size, chaotic transport is enhanced. Incorporating a phase shift into the alternating flow reorients the self-similar structure. It can also control the extent of chaos; compare $\delta \neq 0$ in Figures 4, 5 and 6 for the two different values of K_1. Overall, the figures illustrate an underlying recirculation pattern based on bidirectional flow is more robust to the wall motion than a recirculation pattern based on a constant unidirectional flow (that is, Moffatt flow). Our results have extended earlier work (3) and add further support to the idea that in small airways where the Reynolds number is very low, the interaction between recirculation and wall motion can produce efficient mixing by chaotic advection. Moreover, the model presented here shows that the extent of this chaos is related to the way the basic pattern of recirculation is initially formed, which was not apparent in our earlier model.

Acknowledgements

This research was supported by NIH BRP HL070542, which is a collaborative project led by Akira Tsuda of the Harvard School of Public Health. We are grateful to a referee for some very constructive suggestions that have helped to clarify this work.

References

[1] D. J. Acheson, *Elementary Fluid Dynamics*, Oxford University Press 1990.

[2] S. Haber, J. P. Butler, H. Brenner, I. Emanuel and A. Tsuda, Shear flow over a self-similar expanding pulmonary alveolus during rhymical breathing, *J. Fluid Mech.*, 405:243–268, 2000.

[3] F. E. Laine-Pearson and P. E. Hydon, Particle Transport in a Moving Corner, *J. Fluid Mech.*, 559:379–390, 2006.

[4] A. J. Lichtenberg and M. A. Lieberman, *Regular and Chaotic Dynamics*, Springer-Verlag, second edition, 1992.

[5] H. K. Moffatt, Viscous and resistive eddies near a sharp corner, *J. Fluid Mech.*, 18:1–18, 1964.

[6] H. K. Moffatt and B. R. Duffy, Local similarity solutions and their limitations, *J. Fluid Mech.*, 96:299–313, 1980.

[7] M. Ochs, J. R. Nyengaard, A. Jung, L. Knudsen, M. Voigt, T. Wahlers, J. Richter and H. J. G. Gundersen, The Number of Alveoli in the Human Lung, *Am. J. Respir. Crit. Care Med.*, 169:120–124, 2004.

[8] M. Tabor, *Chaos and Integrability in Nonlinear Dynamics*, Wiley, 1989.

[9] A. Tippe and A. Tsuda, Recirculating flow in an expanding alveolar model: experimental evidence of flow-induced mixing of aerosols in the pulmonary acinus, *J. Aerosol Sci.*, 31(8):979–986, 1999.

[10] A. Tsuda, F. S. Henry and J. P. Butler, Chaotic mixing of alveolated duct flow in rhythmically expanding pulmonary acinus, *J. Appl. Physiol.*, 79:1055–1063, 1995.

[11] A. Tsuda, R. A. Rogers, P. E. Hydon and J. P. Butler, Chaotic mixing deep in the lung, *Proc. Nat. Acad. Sci.*, 19:10173–10178, 2002.